Heliyon 6 (2020) e05391

Contents lists available at ScienceDirect

Heliyon

journal homepage: www.cell.com/heliyon

Research article

Carboxymethyl cellulose-based polyelectrolyte as cationic exchange membrane for zinc-iodine batteries

Phonnapha Tangthuam [a], Jirapha Pimoei [a], Ahmad Azmin Mohamad [b], Falko Mahlendorf [c], Anongnat Somwangthanaroj [a], Soorathep Kheawhom [a,d,*]

[a] Department of Chemical Engineering, Faculty of Engineering, Chulalongkorn University, Bangkok 10330, Thailand
[b] School of Materials and Mineral Resources Engineering, Universiti of Sains Malaysia, Nibong Tebal 14300, Malaysia
[c] Department of Energy Technology, University Duisburg-Essen, Duisburg 47057, Germany
[d] Research Unit of Advanced Materials for Energy Storage, Chulalongkorn University, Bangkok 10330, Thailand

ARTICLE INFO

Keywords:
Chemical engineering
Energy
Materials science
Chemical energy storage
Electrochemical energy engineering
Energy storage technology
Polymers
Electrochemistry
Zinc-iodine battery
Polyiodide crossover
Ionic conductivity
Cationic exchange
Anionic polyelectrolyte

ABSTRACT

The aim of this research is an evaluation of polyelectrolytes. In the application of zinc-iodine batteries (ZIBs), polyelectrolytes have high stability, good cationic exchange properties and high ionic conductivity. Polyelectrolytes are also cost-effective. Important component of ZIBs are cation exchange membranes (CEMs). CEMs prevent the crossover of iodine and polyiodide from zinc (Zn) electrodes. However, available CEMs are costly and have limited ionic conductivity at room temperature. CEMs are low-cost, have high stability and good cationic exchange properties. Herein, polyelectrolyte membranes prepared from carboxymethyl cellulose (CMC) and polyvinyl alcohol (PVA) are examined. It is seen that an increase in the ratio of PVA leads to enhanced ionic conductivity as well as increased iodine and polyiodide crossover. ZIBs using polyelectrolytes having 75:25 wt.% CMC/PVA and 50:50 wt.% CMC/PVA show decent performance and cycling stability. Due to their low-cost and other salient features, CMC/PVA polyelectrolytes prove they have the capacity for use as cation exchange separators in ZIBs.

1. Introduction

Owing to an excess of carbon dioxide (CO_2) in the atmosphere, global environmental issues are becoming progressively stringent (Abbasi et al., 2019b; Apergis et al., 2020; Zhang, 2013). The use of renewable energy sources, therefore, such as solar and wind, are rapidly developing. Renewable energy sources are very intermittent and highly erratic; stabilizing electricity production is becoming demanding (Ghiani and Pisano, 2018; Guo et al., 2020; Li et al., 2020). Effective stabilization in electricity production and utilization can be fulfilled using rechargeable batteries. The demand for large-scale battery systems has increased dramatically. Rechargeable batteries having a large capacity, reliable safety and cost effectiveness are preferred (Frate et al., 2020; Guney and Tepe, 2017; Rancilio et al., 2019).

As their capacity depends on their power, traditional enclosed batteries are seen to have limited potential. Flow batteries, however, can store active material on the outside and can independently scale up the power and capacity of the system (Perry and Weber, 2015). For this reason, flow batteries demonstrate significant advantages over other types of batteries. Existing flow batteries, however, are based on vanadium (V), which is toxic and costly. Therefore, the development of flow batteries that are cheap and eco-friendly is of vital importance (Chen et al., 2018; García-Quismondo et al., 2019).

Nowadays, due to their low-cost, high stability and eco-friendliness, Zn-based aqueous flow batteries are much in demand (Hosseini et al., 2019; Hosseini et al., 2018a,b; Lao-atiman et al., 2019). Among various Zn-based redox chemistries, the iodide/iodine (I^-/I_2) redox couple show the most promise and excellent electrochemical performance. The abundance of iodine in ocean water (50–60 mg/l) meets the need for sustainable energy (Gong et al., 2017). ZIBs exhibit much higher volumetric energy density than other flow battery systems (Mousavi et al., 2020). In Figure 1a, a schematic diagram of a ZIB is shown. ZIBs use iodine solution as an active catholyte and a porous carbon electrode as the cathode. Previous studies suggest that a CEM separator is pivotal in

* Corresponding author.
E-mail address: soorathep.k@chula.ac.th (S. Kheawhom).

https://doi.org/10.1016/j.heliyon.2020.e05391
Received 9 September 2020; Received in revised form 16 October 2020; Accepted 27 October 2020

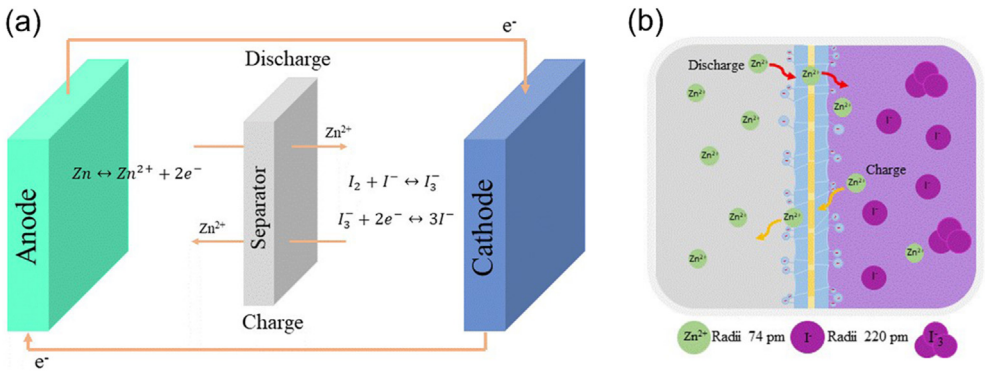

Figure 1. Schematic diagram and functions of CEM separator in ZIBs: (a) Schematic diagram of ZIBs and (b) Functions of CEM separator in ZIBs.

determining the performance of ZIBs (Weng et al., 2017; Xie et al., 2020). As shown in Figure 1b, a CEM separator facilitates the transfer of Zn ions across cells while preventing the crossover of iodine and polyiodide.

One of the most significant obstacles limiting ZIBs from achieving their expected performance is the very high cost of commercial CEMs (Weng et al., 2017; Xie et al., 2019). Subsequently, developments are duly being carried out to produce alternative low-cost CEMs, having excellent chemical resistance, good mechanical stability, and decent ionic conductivity (Bhunia and Dutta, 2018). Anionic polyelectrolytes, which are capable of cation exchange, are favorable alternatives to costly CEMs.

Of the various types of anionic polyelectrolytes, CMCs exhibit great promise due to their biocompatibility, low-cost, and good film-forming ability (Saadiah et al., 2019). A CMC molecule contains fixed negative charge carriers and mobile positive charge carriers (Parman, 1983; Valappil et al., 2013). A CMC molecule can also form a complex with some salts, resulting in the enhancement of ionic conductivity (Isa and Samsudin, 2016). CMCs have been applied in various applications such as superabsorbent hydrogel skin-protection and biopolymer electrolytes (Gao et al., 2017; Shin et al., 2020). Mechanical properties of CMCs can be improved by blending with other polymers. PVA is an interesting polymer for blending with CMCs due to its prominent advantage of a physical crosslinking between hydroxyl groups (Gao et al., 2017; Kumar et al., 2019). However, studies on the application of CMCs and PVA polyelectrolytes in ZIBs have not been properly addressed. The cation exchange property of CMC for use as a low-cost separator in ZIBs and other batteries shows promise.

A Zn-iodine flow battery (ZIFB) was first demonstrated by the PNNL National Laboratory at Northwestern University (Li et al., 2015). The ZIFB exhibited excellent performance delivering a volumetric energy density of 167 Wh/l, which is close to the energy density of common lithium-ion batteries (LIBs). Weng et al. (2017) reported another ZIFB system using bromide ions as a complexing agent to stabilize free iodine in the electrolyte, improving energy density even more. ZIFBs, however, are still limited on account of their short cycle life (<50 cycles), low current density (<10 mA cm^{-2}), and relatively high cost, resulting from the costly Nafion membrane (500–700 $ m^{-2}). Both the low conductivity of electrolytes and the low ionic conductivity of the Nafion membrane, in a neutral electrolyte, can lead to low discharge current densities of ZIFBs (Yuan et al., 2016).

In this work, rechargeable ZIBs using polyelectrolyte membrane separators, having different ratios of CMC/PVA, are investigated. Graphite felt, having a highly porous architecture, is used as the positive electrode. As for the negative electrode, Zn electrodeposited on graphite felt is employed. Detailed material and methods can be found in the accompanying supplemental file (Supplemental_Information.docx). Results highlight the capability of CMC/PVA polyelectrolytes for use as CEM separators in ZIBs. The effects of the ratios of CMC/PVA on performance of ZIB are studied.

2. Results and discussion

The structures of CMC and PVA were investigated via Fourier Transform Infrared Spectroscopy (FTIR). In Figures. 2a and b, the FTIR spectra of CMC and PVA are presented. At 1065 cm^{-1}, 1326 cm^{-1}, 1417 cm^{-1}, 1603 cm^{-1} and 3442 cm^{-1}, corresponding to C-O-C bonding, O-H bonding, -CH_2 scissoring, COO- asymmetric and -OH stretching, the absorption bands of CMC can be seen. These results were found to be in good agreement with those reported by Saadiah et al., confirming the presence of cellulose and carboxymethyl groups which are the backbone of CMC (Saadiah et al., 2019). At 849 cm^{-1}, 1093 cm^{-1}, 1376 cm^{-1} and 3326 cm^{-1}, corresponding to C-C bonding, C-O stretching, C-H wagging, and -OH stretching, the absorption bands of PVA can be observed. In addition, the absorption bands in the range: 1065 - 1376 cm^{-1} represent the vibration of the carbon skeletal of the cellulose backbone structure (El-Sawy et al., 2010).

According to Riaz and Ashraf (2014), the mechanical properties of a polymer blend are directly related to the molecular chain between the constituent polymers and their miscibility, in which interaction between the functional groups in the polymer blend could be observed via FTIR. The properties of a homogeneous blend are often an arithmetical average of the properties of each component whilst the miscibility of the components is usually caused by the formation of hydrogen bonds. The common complexation between CMC and PVA is through hydrogen bonding. Hydrogen bonding is an important factor which affects the crystalline nature of the polymer (Dias et al., 2011).

As shown in Figure 2b, the absorption bands in the region of 3400 cm^{-1} represent all types of hydrogen bonds (-OH groups). Meanwhile, the peaks shifted their position due to the process of complexation. In the CMC-PVA blend, the peaks of the pure CMC: 1065 cm^{-1}, 1326 cm^{-1}, 1417 cm^{-1} and 1603 cm^{-1} shifted position slightly as follows: 1059 cm^{-1}, 1314 cm^{-1}, 1413 cm^{-1} and 1619 cm^{-1}. In addition, the peaks of the pure PVA: 849 cm^{-1}, 1093 cm^{-1} and 1376 cm^{-1} also shifted position slightly: 849 cm^{-1}, 1106 cm^{-1} and 1382 cm^{-1}.

As illustrated in Figures. 3a and b, the new shoulder of absorption regions appear at 849 cm^{-1} and 1714 cm^{-1} in C25. These regions represent C-C of PVA. When CMC was added, the intensities of the absorption peaks of PVA i.e. 849 cm^{-1}, 1382 cm^{-1}, 1714 cm^{-1} and 2942 cm^{-1} decreased. Some peaks, however, disappeared such as the pure CMC peak at 2930 cm^{-1} (C-H) and the pure PVA peak at 1259 cm^{-1} (-OH). Shin et al. (2020) reported that the FTIR spectra of PVA/CS (chitosan) polymer blend at 1255 cm^{-1} disappeared (-OH of pure PVA) and that hydrogen bonds formed between PVA and CS.

In Figure 3a, the interaction between CMC and PVA molecules is presented. At wavenumbers 1059 cm^{-1} to 1106 cm^{-1}, a band appeared which is attributed to ether linkage (C-O-C), consisting of an oxygen site that could form intermolecular hydrogen bonding with other molecules. In Figure 3b, the peaks in the region between 1314-1619 cm^{-1} can be seen to correspond to the carboxylate and hydroxyl groups where the

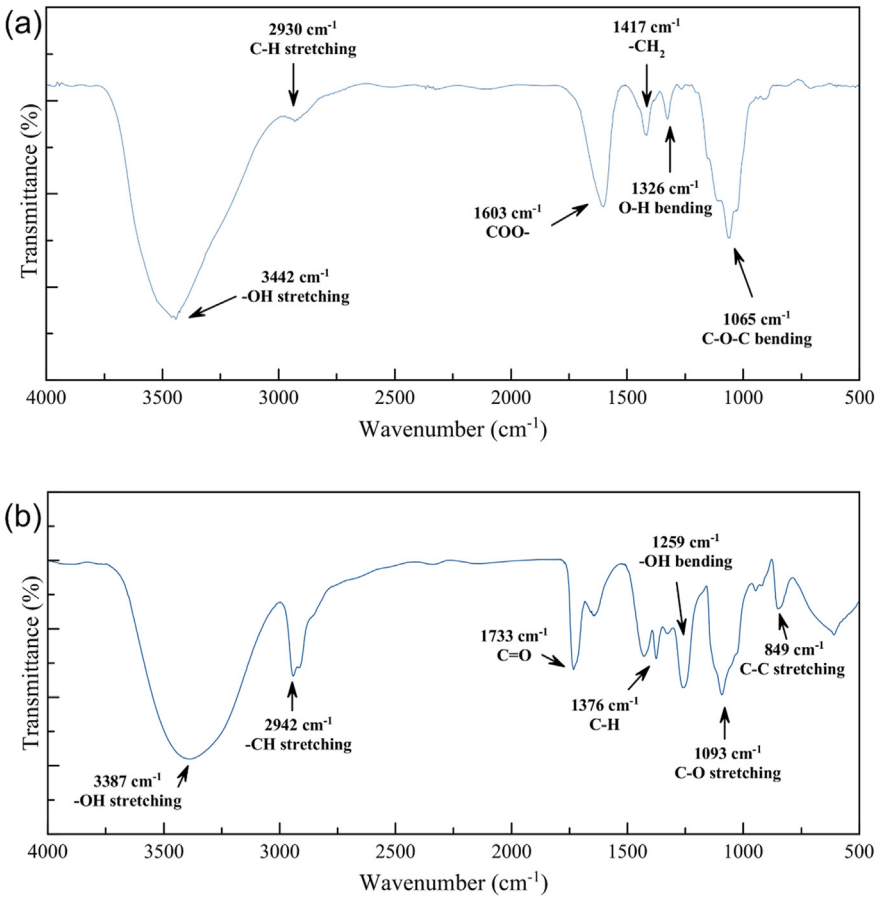

Figure 2. FTIR spectra of (a) Pure CMC and (b) Pure PVA.

intensity of both peaks increased, as the ratio of CMC increased. Intermolecular hydrogen bonding for the CMC/PVA system occurs at the region assigned to the bonding of -OH and -COO functional groups for the complexation (Saadiah et al., 2019). In Figure 3c, it was noted that the addition of CMC led to the formation of hydrogen bonds of the hydroxyl groups, as crosslinking increased; thus, the absorption bands in the region 3200-3500 cm^{-1} were seen to get wider (Shin et al., 2020). Besides, at 2942 cm^{-1}, a small peak is seen which represents -CH stretching. Consequently, C75 showed significant changes because the highest interaction occurred between CMC and PVA.

As shown in Figure 4, SEM images of the surface morphology of the polyelectrolyte membranes are shown. It can be observed that the surfaces of the images C25, C50 and C75 are not smooth and each structure is very flaky. Apparently, the polyelectrolyte membranes, having a higher ratio of CMC, exhibit a flaky structure and smaller sized pores. The more compact morphology and lesser pore structure act as a barrier to water

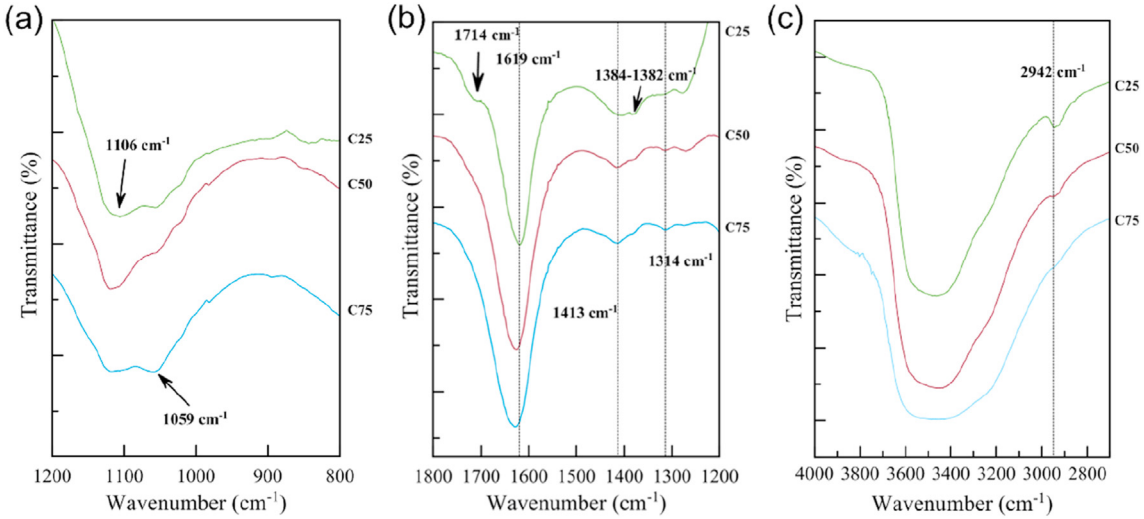

Figure 3. FTIR spectra for CMC/PVA polyelectrolytes in wavenumbers of: (a) 800-1200 cm^{-1} (b) 1200-1800 cm^{-1} and (c) 2800-4000 cm^{-1}

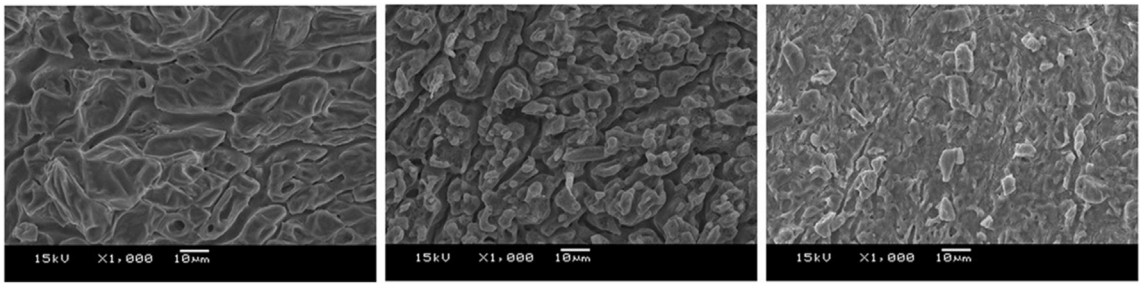

Figure 4. SEM images of C25, C50 and C75 (from left to right).

diffusion (Handaya Saputra and Huda Apriliana, 2018). In comparison, C25 had larger pores and a less compact structure.

The ionic conductivity of each polyelectrolyte membrane was determined via EIS (Abbasi et al., 2019a). In Figure 5a, the ionic conductivity of the membrane as a function of CMC ratio is shown. It is noted that the ionic conductivity of C25 was higher than the others. In contrast, C75 exhibited the lowest ionic conductivity. The ionic conductivities of C25, C50, and C75 are as follows: 119.8 mS/cm^2, 93.5 mS/cm^2, and 48.7 mS/cm^2, respectively. In Figure 5b, the trend of iodine and polyiodide crossover of each membrane is presented. It was found that the iodine and polyiodide crossover exhibited a similar trend to the ionic conductivity. C75 demonstrated the lowest iodine and polyiodide crossover, indicating the highest iodine blocking effect.

It is acknowledged that PVA consists of hydroxyl groups that provide hydrogen bonding with CMC and water. These hydroxyl groups of PVA can absorb a large amount of water and hence encourage ionic conductivity (Alipoori et al., 2020). In the case of C75, the movement of ions through the membrane was beset by obstacles because the cation-exchange property of CMC only allowed cations to penetrate through the membrane, preventing other species. However, the membrane in all cases could not totally prevent the iodine and polyiodide crossover because iodine molecules could pass through the membrane via different mechanisms (Svensson and Kloo, 2003). During the long-term experiment, the leaking of a small amount of iodine to the anolyte could be observed.

In Figure 6a, the discharge polarization of ZIBs using C25, C50 and C75 is shown. In all cases, the batteries indicated ohmic polarization characteristic, which was dominated by the internal resistance, as contributed by the separator, electrode, and current collector. In determining battery performance, ionic conductivity plays an important role. A battery using a membrane having high ionic conductivity could discharge at a higher voltage. The ionic conductivity of polyelectrolytes strongly affects internal resistance and can determine the performance of the batteries. Although C25 exhibited the highest ionic conductivity as well as the highest battery performance, its poor iodine and polyiodide crossover raised concern about its long-term stability. C25 was excluded, therefore, from the galvanostatic charge-discharge cycling test.

In Figure 6b, the galvanostatic charge-discharge cycling of ZIBs using C50 and C75 is presented. As shown in Figure 6b, both charge and discharge voltages follow the trend of ionic conductivity. Due to their galvanostatic cycling performance, the C50 and C75 cells provided excellent reversibility; cycle life reached more than 300 cycles. During the long-term cycling, discharge voltage dropped slightly, and charge voltage increased just a little. In Figure 6c, at the 1st cycle, the voltage gap between charge and discharge of the C50 and C75 cells was found to be 0.485 V and 0.648 V, respectively. This voltage gap occurred as a result of the iodine and polyiodide crossover, which increased through time. In Figure 6d, at the 90th cycle, the voltage gap of the C50 cell increased to 0.569 V, exhibiting a 17.32% increase in voltage gap. In contrast, the voltage gap of the C75 cell decreased slightly to 0.645 V, a decrease of 0.46%. Consequently, C75 demonstrated higher stability. The high stability of the C75 cell was due to the smaller iodine and polyiodide crossover during the long-term cycling.

The stability of the C75 membrane was further studied via FTIR. In Figure 7, the spectra for the membrane sample immersed in 0.5 N iodine solution (10 ml), at different periods of time (0–24 h), can be observed. Previous studies on the spectrum band of alkyl halide reported that alkyl halide vibration frequencies appeared in the region 550-850 cm^{-1} (Coates, 2006; Vidya and Nikhil, 2016). Alkyl halides are compounds in which one or more hydrogen atoms have been substituted by halogen atoms. The absorption band at 490-620 cm^{-1} is attributed to halogen compounds viz. C-I stretching (Coates, 2006). Owing to the different electronegativity between the halogen and carbon atoms, the C-halogen bonds were found to be polar. However, in the case of the C-I bond, the electronegativity between carbon and iodine were found to be similar, forming temporary dipoles between carbon and iodine. This outcome led to a weak bond between carbon and iodine atoms. In the polymeric chain, iodine atoms were seen to migrate and bond together with different carbon atoms.

In Figure 7a, a peak appeared at around 612 cm^{-1} together with another small peak at 571 cm^{-1}, corresponding to the alkyl halide which

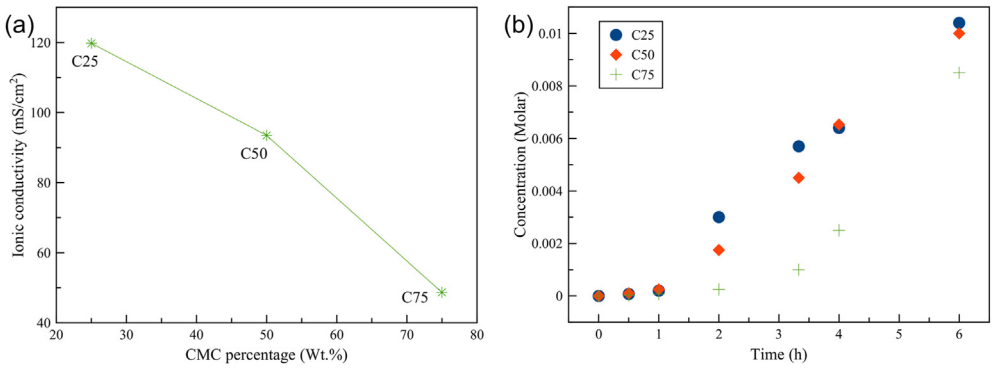

Figure 5. Ionic conductivity and iodine and polyiodide crossover of different polyelectrolyte membranes: (a) Ionic conductivities of C25, C50 and C75 and (b) Iodine and polyiodide crossover of C25, C50 and C75.

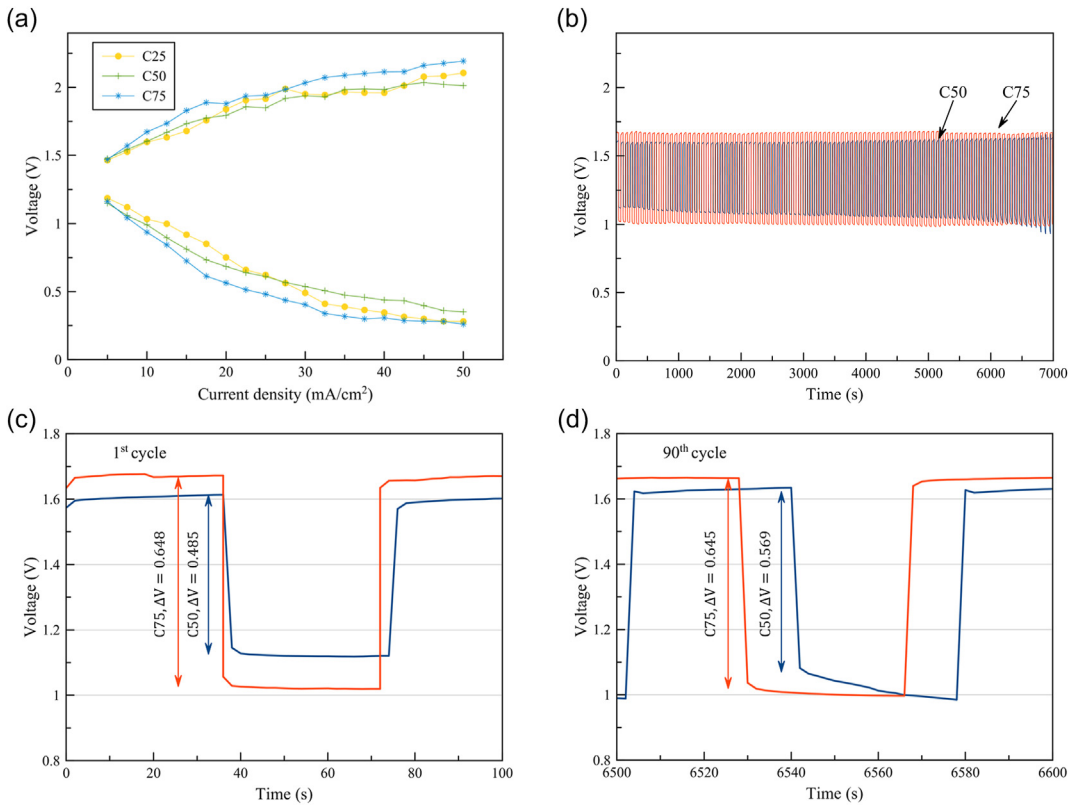

Figure 6. Electrochemical performances of ZIBs using different polyelectrolyte membranes: (a) Polarization of the voltage with respect to the current density 5–50 mA/cm^2 (b) Galvanostatic cycling test of C50 and C75 battery at current density 10 mA/cm^2 (c) Galvanostatic cycling test from 0-100 s and (d) Galvanostatic cycling test from 4900-5000 s.

suddenly developed after the membrane was immersed in iodine longer than 6 h. Results demonstrated that iodo compounds occurred in the system. As for the band region viz. 1150-1300 cm^{-1}, this region corresponded to C-H wagging, in the presence of alkyl halides. Meanwhile, the spectrum peak at 984 cm^{-1} is attributed to the C-H stretching vibration. The phenomenon of the alkyl halogen relates to the crossover of iodine and polyiodide in the system after the C75 membrane had been immersed in iodine for a long time. Results revealed that the crossover of the iodine and polyiodide was due to the appearance of the alkyl halide in the CMC/PVA polyelectrolyte membrane system.

Zhang et al. (2018) reported that a ZIB exhibited a significantly high discharge voltage i.e.1.47V at 10 mA/cm^2, as the anolyte contained alkaline solution. This outcome occurred due to the dissolution of Zn in an alkaline solution, resulting in a more negative potential than in an

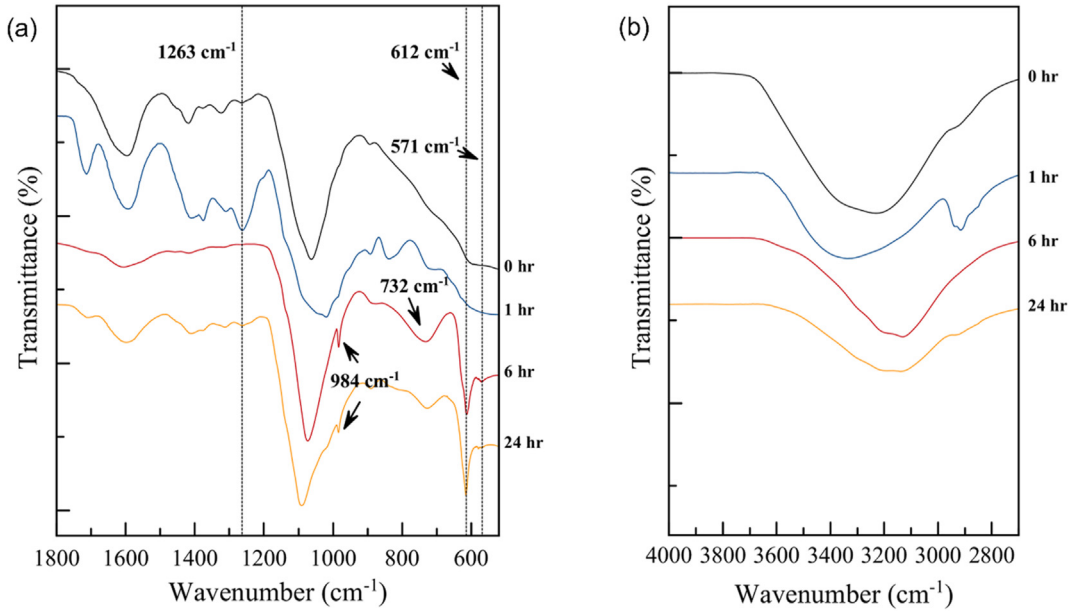

Figure 7. FTIR spectra for the hydrogel membrane immersed in iodine electrolyte in wavenumbers: a) 500-1800 cm^{-1} and b) 2800-4000 cm^{-1}

acidic solution. Nafion 117 was used as separator. However, the use of polyelectrolyte membranes in the system having alkaline anolytes must be examined further. Li et al. (2015) reported that the discharge voltage exhibited 1.10V at 10 mA/cm^2 in the ZnI_2 electrolyte system and used Nafion 115 as the separator. As observed, the above results differed due to the various parameters used: electrolyte, negative electrode, current collector, separator, and cell configuration. As for the positive electrode, all works used graphite felt. The ZIBs which used CMC/PVA polyelectrolyte membranes exhibited comparable performances: namely, 1.12 discharge voltage (C50) and 1.02 discharge voltage (C75). Hence, the CMC/PVA membranes proved to have a competitive cost advantage. When employed on a large-scale, this cost-benefit can be in their favor. Based on their excellent ionic conductivity and decent stability, CMC/PVA polyelectrolytes can be considered as promising CEM separators for ZIBs.

3. Conclusion

This paper investigated the effect of polyelectrolyte membranes, having different ratios of CMC/PVA, for use as CEM separators in ZIBs. It is evident that the polyelectrolyte membranes were found to prevent the crossover of both iodine and polyiodide. Besides, the increase in ratio of CMC in the separator provided greater cationic exchange property. The ionic conductivity of the polyelectrolyte membranes is proportionally related to the ratio of PVA. Nevertheless, the membranes having higher ionic conductivity exhibited higher iodine and polyiodide crossover. Though C25 demonstrated the highest ionic conductivity having 1.12V discharge at 10 mA/cm^2, its high iodine and polyiodide crossover raised concern regarding its long-term stability. The ZIBs using C50 and C75 membranes displayed acceptable charge-discharge performance and good cycling stability. CMC/PVA polyelectrolytes show high potential as low-cost CEM separators for ZIBs. This concept can be extended to other types of battery that require cation exchange properties.

3.1. Limitations of the study

The zinc-iodine batteries proposed here still suffer from a small amount of iodine and polyiodide crossover, reflecting their long-term stability. A further in-depth study about the mechanism of iodine migration in different polyelectrolytes, as well as its kinetics, might afford a more effective iodine blocking. In addition, performance of the cells was examined using a static H-cell instead of a flow battery. Thus, implementation of the polyelectrolytes in a flow battery configuration is essential to evaluate their practical potential in ZIBs.

Declarations

Author contribution statement

Phonnapha Tangthuam: Conceived and designed the experiments; Performed the experiments; Analyzed and interpreted the data; Wrote the paper.

Jirapha Pimoei: Performed the experiments.

Ahmad Azmin Mohamad & Falko Mahlendorf: Analyzed and interpreted the data; Wrote the paper.

Anongnat Somwangthanaroj & Soorathep Kheawhom: Conceived and designed the experiments; Analyzed and interpreted the data; Contributed reagents, materials, analysis tools or data; Wrote the paper.

Funding statement

This work was supported by Global Partnership Funding (B16F630071), and the Energy Storage Cluster, Chulalongkorn University. Phonnapha Tangthuam was supported by Chulalongkorn Academic Advancement into its Second Century Project: C2F PhD Fellowship.

Competing interest statement

The authors declare no conflict of interest.

Additional information

Supplementary content related to this article has been published online at https://doi.org/10.1016/j.heliyon.2020.e05391.

References

Abbasi, A., Hosseini, S., Somwangthanaroj, A., Mohamad, A.A., Kheawhom, S., 2019a. Poly(2,6-Dimethyl-1,4-Phenylene oxide)-based hydroxide exchange separator membranes for zinc–air battery. Int. J. Mol. Sci. 20, 3678.

Abbasi, A., Nasef, M.M., Babadi, F.E., Faridi-Majidi, R., Takeshi, M., Abouzari-Lotf, E., Choong, T., Somwangthanaroj, A., Kheawhom, S., 2019b. Carbon dioxide adsorption on grafted nanofibrous adsorbents functionalized using different amines. Front. Energy Res. 7.

Alipoori, S., Mazinani, S., Aboutalebi, S.H., Sharif, F., 2020. Review of PVA-based gel polymer electrolytes in flexible solid-state supercapacitors: opportunities and challenges. J. Energy Storage 27, 101072.

Apergis, N., Payne, J.E., Rayos-Velazquez, M., 2020. Carbon dioxide emissions intensity convergence: evidence from central American countries. Front. Energy Res. 7.

Bhunia, P., Dutta, K., 2018. Chapter 16 - biochemistry and Electrochemistry at the electrodes of microbial fuel cells. In: Kundu, P.P., Dutta, K. (Eds.), Progress and Recent Trends in Microbial Fuel Cells. Elsevier, pp. 327–345.

Chen, H., Cong, G., Lu, Y.-C., 2018. Recent progress in organic redox flow batteries: active materials, electrolytes and membranes. J. Energy Chem. 27, 1304–1325.

Coates, J., 2006. Interpretation of infrared spectra, A practical approach. In: Encyclopedia of Analytical Chemistry.

Dias, L.L.S., Mansur, H.S., Donnici, C.L., Pereira, M.M., 2011. Synthesis and characterization of chitosan-polyvinyl alcohol-bioactive glass hybrid membranes. Biomatter 1, 114–119.

El-Sawy, N.M., El-Arnaouty, M.B., Ghaffar, A.M.A., 2010. γ-Irradiation effect on the non-cross-linked and cross-linked polyvinyl alcohol films. Polym. Plast. Technol. Eng. 49, 169–177.

Frate, G.F., Ferrari, L., Desideri, U., 2020. Multi-criteria economic analysis of a pumped thermal electricity storage (PTES) with thermal integration. Front. Energy Res. 8.

Gao, Z., Yu, Z., Huang, C., Duan, L., Gao, G.H., 2017. Carboxymethyl cellulose reinforced poly(vinyl alcohol) with trimethylol melamine as a chemical crosslinker. J. Appl. Polym. Sci. 134.

García-Quismondo, E., Almonacid, I., Cabañero Martínez, M.Á., Miroslavov, V., Serrano, E., Palma, J., Alonso Salmerón, J.P., 2019. Operational experience of 5 kW/5 kWh all-vanadium flow batteries in photovoltaic grid applications. Batteries 5, 52.

Ghiani, E., Pisano, G., 2018. Chapter 2 - impact of renewable energy sources and energy storage technologies on the operation and planning of smart distribution networks. In: Zare, K., Nojavan, S. (Eds.), Operation of Distributed Energy Resources in Smart Distribution Networks. Academic Press, pp. 25–48.

Gong, D., Wang, B., Zhu, J., Podila, R., Rao, A.M., Yu, X., Xu, Z., Lu, B., 2017. An iodine quantum dots based rechargeable sodium–iodine battery. Adv. Energy Mater. 7, 1601885.

Guney, M.S., Tepe, Y., 2017. Classification and assessment of energy storage systems. Renew. Sustain. Energy Rev. 75, 1187–1197.

Guo, Z., Zhang, X., Feng, S., Zhang, H., 2020. The impacts of reducing renewable energy subsidies on China's energy transition by using a hybrid dynamic computable general equilibrium model. Front. Energy Res. 8.

Handaya Saputra, A., Huda Apriliana, N., 2018. Polyvinyl alcohol (PVA) partially hydrolyzed addition in synthesis of natural hydrogel carboxymethyl cellulose (CMC) based from water hyacinth. MATEC Web Conf. 156, 01007.

Hosseini, S., Abbasi, A., Uginet, L.-O., Haustraete, N., Praserthdam, S., Yonezawa, T., Kheawhom, S., 2019. The influence of dimethyl sulfoxide as electrolyte additive on anodic dissolution of alkaline zinc-air flow battery. Sci. Rep. 9, 14958.

Hosseini, S., Han, S.J., Arponwichanop, A., Yonezawa, T., Kheawhom, S., 2018a. Ethanol as an electrolyte additive for alkaline zinc-air flow batteries. Sci. Rep. 8, 11273.

Hosseini, S., Lao-atiman, W., Han, S.J., Arpornwichanop, A., Yonezawa, T., Kheawhom, S., 2018b. Discharge performance of zinc-air flow batteries under the effects of sodium dodecyl sulfate and pluronic F-127. Sci. Rep. 8, 14909.

Isa, M.I.N., Samsudin, A.S., 2016. Potential study of biopolymer-based carboxymethylcellulose electrolytes system for solid-state battery application. Int. J. Polymeric Mater. Polyme. Biomat. 65, 561–567.

Kumar, S., Prajapati, G.K., Saroj, A.L., Gupta, P.N., 2019. Structural, electrical and dielectric studies of nano-composite polymer blend electrolyte films based on (70–x) PVA–x PVP–NaI–SiO2. Phys. B Condens. Matter 554, 158–164.

Lao-atiman, W., Bumroongsil, K., Arpornwichanop, A., Bumroongsakulsawat, P., Olaru, S., Kheawhom, S., 2019. Model-based analysis of an integrated zinc-air flow battery/zinc electrolyzer system. Front. Energy Res. 7, 15.

Li, B., Nie, Z., Vijayakumar, M., Li, G., Liu, J., Sprenkle, V., Wang, W., 2015. Ambipolar zinc-polyiodide electrolyte for a high-energy density aqueous redox flow battery. Nat. Commun. 6, 6303.
Li, Y., Wang, C., Li, G., 2020. A mini-review on high-penetration renewable integration into a smarter grid. Front. Energy Res. 8.
Mousavi, M., Jiang, G., Zhang, J., Kashkooli, A.G., Dou, H., Silva, C.J., Cano, Z.P., Niu, Y., Yu, A., Chen, Z., 2020. Decoupled low-cost ammonium-based electrolyte design for highly stable zinc–iodine redox flow batteries. Energy Storage Mater. 32, 465–476.
Parman, A.Ü., 1983. Comparison of carboxymethyl-cellulose cation-exchange chromatography and high-performance liquid chromatography in the purification of Guinea-pig insulin from pancreatic extracts. J. Chromatogr. A 256, 293–301.
Perry, M.L., Weber, A.Z., 2015. Advanced redox-flow batteries: a perspective. J. Electrochem. Soc. 163, A5064–A5067.
Rancilio, G., Lucas, A., Kotsakis, E., Fulli, G., Merlo, M., Delfanti, M., Masera, M., 2019. Modeling a large-scale battery energy storage system for power grid application analysis. Energies 12, 3312.
Riaz, U., Ashraf, S.M., 2014. Characterization of polymer blends with FTIR spectroscopy. Characterization of Polymer Blends, pp. 625–678.
Saadiah, M.A., Zhang, D., Nagao, Y., Muzakir, S.K., Samsudin, A.S., 2019. Reducing crystallinity on thin film based CMC/PVA hybrid polymer for application as a host in polymer electrolytes. J. Non-Cryst. Solids 511, 201–211.
Shin, J.-Y., Lee, D.Y., Yoon, J.I., Song, Y.-S., 2020. Effect of CMC concentration on cell growth behavior of PVA/CMC hydrogel. Macromol. Res. 28, 813–819.
Svensson, P.H., Kloo, L., 2003. Synthesis, structure, and bonding in polyiodide and metal Iodide−Iodine systems. Chem. Rev. 103, 1649–1684.
Valappil, S.P., Yiu, H.H.P., Bouffier, L., Hope, C.K., Evans, G., Claridge, J.B., Higham, S.M., Rosseinsky, M.J., 2013. Effect of novel antibacterial gallium-carboxymethyl cellulose on Pseudomonas aeruginosa. Dalton Trans. 42, 1778–1786.
Vidya, K., Nikhil, G., 2016. Fourier Transform infrared spectroscopy spectroscopic studies in embelia ribes burm. F.: a vulnerable medicinal plant. Asian J. Pharmaceut. Clin. Res. 9.
Weng, G.-M., Li, Z., Cong, G., Zhou, Y., Lu, Y.-C., 2017. Unlocking the capacity of iodide for high-energy-density zinc/polyiodide and lithium/polyiodide redox flow batteries. Energy Environ. Sci. 10, 735–741.
Xie, C., Li, T., Deng, C., Song, Y., Zhang, H., Li, X., 2020. A highly reversible neutral zinc/manganese battery for stationary energy storage. Energy Environ. Sci. 13, 135–143.
Xie, C., Liu, Y., Lu, W., Zhang, H., Li, X., 2019. Highly stable zinc–iodine single flow batteries with super high energy density for stationary energy storage. Energy Environ. Sci. 12, 1834–1839.
Yuan, Z., Duan, Y., Zhang, H., Li, X., Zhang, H., Vankelecom, I., 2016. Advanced porous membranes with ultra-high selectivity and stability for vanadium flow batteries. Energy Environ. Sci. 9, 441–447.
Zhang, J., Jiang, G., Xu, P., Ghorbani Kashkooli, A., Mousavi, M., Yu, A., Chen, Z., 2018. An all-aqueous redox flow battery with unprecedented energy density. Energy Environ. Sci. 11, 2010–2015.
Zhang, S., 2013. Status, opportunities, and challenges of electrochemical energy storage. Front. Energy Res. 1.